Steel and Composite Structures, *Vol. 31*, *No. 1* (*2019*) *53-67*
DOI: https://doi.org/10.12989/scs.2019.31.1.053

Numerical simulation of Y-type perfobond rib shear connectors using finite element analysis

Kun-Soo Kim [1], Oneil Han [2], Munkhtulga Gombosuren [2] and Sang-Hyo Kim [*2]

[1] *Structural and Seismic Safety Research Team*, *Korea Atomic Energy Research Institute*, *Daedeok-daero 989-111*, *Yuseong-gu*, *Daejeon 34057*, *Republic of Korea*
[2] *School of Civil and Environmental Engineering*, *Yonsei University*, *Yonsei-Ro 50*, *Seodaemun-Gu*, *Seoul 03722*, *Republic of Korea*

(*Received March 20, 2018, Revised December 12, 2018, Accepted March 18, 2019*)

Abstract. This study presents finite element analysis (FEA) on a Y-type perfobond rib shear connection using Abaqus software. The performance of a shear connection is evaluated by conducting a push-out test. However, in practice, it is inefficient to verify the performance by conducting a push-out test with regard to all design variables pertaining to a shear connector. To overcome this problem, FEA is conducted on various shear connectors to accurately estimate the shear strength of the Y-type perfobond rib shear connection. Previous push-out test results for 14 typical push-out test specimens and those obtained through FEA are compared to analyze the shear behavior including consideration of the design variables. The results show that the developed finite element model successfully reflects the effects of changes in the design variables. In addition, using the developed FEA model, the shear resistance of a stubby Y-type perfobond rib shear connector is evaluated based on the concrete strength and transverse rebar size variables. Then, the existing shear resistance formula is upgraded based on the FEA results.

Keywords: Y-type perfobond rib shear connection; shear behavior; finite element analysis; numerical simulation

1. Introduction

A steel–concrete composite structure has superior economic feasibility and structural performance. To maintain the composite action, it is necessary to install a shear connector to counter the shear force at the interface between the steel and concrete parts. Different types of shear connectors have been developed, such as the stud (Viest 1956), perfobond (Leonhardt *et al*. 1987), Y-type perfobond (Kim *et al*. 2013), and composite dowel (Hechler *et al*. 2011) types, which have been widely applied in the construction field. According to Eurocode-4 (CEN 2004), which provides guidelines for the design of shear connectors, performing a push-out test is necessary to verify the structural performance of a shear connector.

Recently, several studies analyzed the composite action by performing a push-out test on shear connectors. However, it is inefficient to verify all the effects of different variables through experiments in terms of time and cost. To overcome this problem, a push-out test was performed using finite element analysis (FEA). To obtain similar results as those obtained via the push-out test on shear connectors, the material nonlinearity, geometric nonlinearity, and contact conditions between the parts should be considered in the FEA.

In recent years, a push-out test simulation using commercial software has been widely performed with the advancement of various modeling techniques. Several studies were conducted on stud-type shear connectors using FEA. Nguyen and Kim conducted a push-out test using FEA on a large stud-type shear connector, the diameters of which were 19, 25, 27, and 30 mm. The failure mode of the studs was verified using a ductile damage for a more accurate numerical simulation (Nguyen and Kim 2009).

Furthermore, a parametric study was conducted on a prestressed concrete spliced girder, which was longitudinally connected using stud-type shear connectors (Kim and Nguyen 2010). Qureshi *et al*. (2011a, b) performed a parametric study considering certain variables, such as the stud location, with respect to the behavior of a stud installed along with a profiled sheet. Xu *et al*. (2012) conducted an experiment and a numerical analysis on the combined effect of studs. They analyzed the shear capacity with consideration of the following variables: shank diameter, stud height, and lateral load. They compared various design codes. Pavlović *et al*. (2013) and Dai *et al*. (2015) performed FEA on a bolted shear connector and a demountable stud, respectively. In other studies, FEA was conducted on different types of shear connectors apart from studs. Oguejiofor and Hosain conducted FEA on perfobond ribs for the first time (1997). Qi *et al*. (2017) proposed FEM model and theoretical formula for studs to investigate the effect of damage degree and location, and performed a parametric study in the various damage degree and location based on the suggested FEM model.

Since then, Al-Darzi *et al*. (2007) performed a

∗Corresponding author, Professor,
E- mail: sanghyo@yonsei.ac.kr

http://www.techno-press.org/?journal=scs&subpage=6 ISSN: 1229-9367 (Print), 1598-6233 (Online)

parametric study considering variables, such as the height and thickness of the ribs and transverse rebar. Zheng *et al.* (2016a) analyzed the shear behavior with consideration of a dowel-hole-shaped perfobond. A theoretical model and analytical formula were suggested to investigate the load–slip relationship (Zheng *et al.* 2016b). Classen and Herbrand conducted FEA of the push-out test using a composite dowel to analyze the concrete crack patterns and shear mechanism (2015).

In addition, Maleki and Bagheri (2008) conducted FEA on channel-type shear connectors. Titoum *et al.* (2016) performed FEA on I-shaped shear connectors. Khorramian *et al.* (2017) performed the push-out tests for two different tilted angle connectors. A nonlinear finite element model was proposed to validate the experiment data. Based on the numerical model, a parametric study was performed depending on the variations in concrete strength and connector's diameters. A Y-type perfobond rib shear connector was developed to simplify the layout of the transverse rebar in flat-type perfobond rib shear connectors. Various types of push-out tests were conducted while considering design variables such as concrete compressive strength (Kim *et al.* 2013, 2015), transverse rebar strength (Kim *et al.* 2018a), horizontal spacing of two row ribs (Kim *et al.* 2018b), and different types of ribs (Kim *et al.* 2013, 2014b, 2017a).

Furthermore, various experimental studies have been conducted that extended beyond the composite-beam test (Kim *et al.* 2014a). The push-out test was also performed to examine the performance of the stubby Y-type perfobond rib shear connector, which is smaller than the conventional Y-type perfobond rib shear connector (Kim *et al.* 2017b). The hysteresis behavior of the stubby Y-type perfobond rib shear connector was analyzed (Kim *et al.* 2017c), and the hysteretic performance was estimated depending on the diameters of transverse rebars (Kim *et al.* 2019). However, an FEA technique that accurately represents the push-out test has not been developed. In this study, an FEA model was developed using Abaqus software (Abaqus 2012) to perform efficient numerical simulations in terms of time and cost effectiveness, while accurately representing the push-out test behavior of a Y-type perfobond rib shear connector. In addition, a parametric study on the stubby Y-type perfobond rib shear connector was conducted by using FEA, and a new shear resistance formula for the stubby type shear connector is suggested by employing the existing formula (Kim *et al.* 2015).

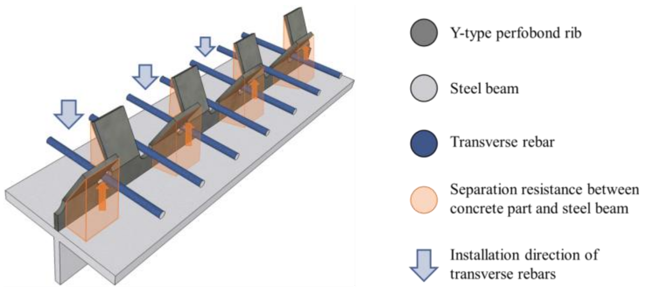

Fig. 1 Characteristics of the Y-type perfobond rib

2. Summary of push-out test of Y-type perfobond rib shear connectors

Kim *et al.* developed Y-type perfobond rib shear connectors (2013). The Y-type perfobond rib shear connectors are characterized by a Y shape cut and an open upper part for easy reinforcement of the transverse rebar, as shown in Fig. 1 (Kim *et al.* 2013, 2016). The rib, which is cut such that it is crossed in both directions, acts as an

Table 1 Variable conditions used in previously conducted typical push-out tests

Specimen	Concrete strength (MPa)	Rib thickness (mm)	Rib width (mm)	Rib height (mm)	Transverse rebar diameter (mm)	Ref.
C40-T10-W80-H100-D16*	40	10	80	100	16	Kim *et al.* (2013)
C40-T10-W80-H100-D0*	40	10	80	100	-	
C40-T8-W80-H100-D16*	40	8	80	100	16	
C30-T10-W80-H100-D16*	30	10	80	100	16	
C40-T10-W60-H100-D16**	40	10	60	100	16	Kim *et al.* (2014b)
C40-T10-W80-H100-D16**	40	10	80	100	16	
C40-T10-W100-H100-D16**	40	10	100	100	16	
C40-T10-W120-H100-D16**	40	10	120	100	16	
C40-T10-W80-H80-D16**	40	10	80	80	16	
C40-T10-W80-H120-D16**	40	10	80	120	16	
C40-T12-W80-H100-D16*	40	12	80	100	16	
C50-T10-W80-H100-D16*	50	10	80	100	16	Kim *et al.* (2015)
C40-T10-W80-H100-D13*	40	10	80	100	13	Kim *et al.* (2017a)
C40-T10-W80-H100-D19*	40	10	80	100	19	

* Specimen with eight ribs; **Specimen with four ribs

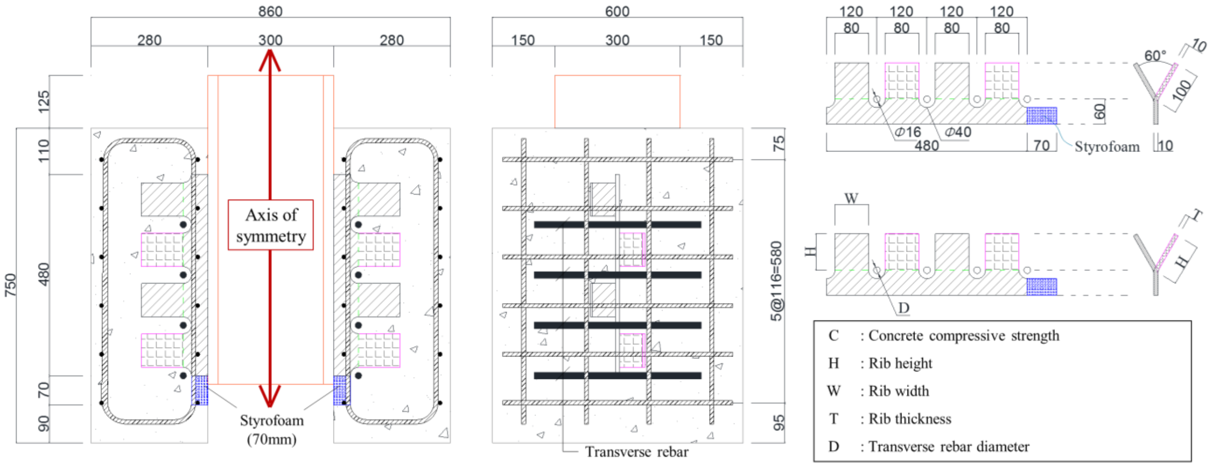

Fig. 2 Layout and design variables of the push-out specimen (unit: mm)

anchor embedded in the concrete. Thus, it helps prevent the separation of the steel part from the concrete part. To improve the ineffective reinforcement method of the transverse rebar in conventional perfobond rib shear connectors, wherein the transverse rebar is reinforced by directly inserting it into a dowel hole, the Y-type perfobond rib shear connectors are designed to conveniently arrange the transverse rebar through the open space in the upper area. Furthermore, the following equation was proposed to estimate the shear strength via the push-out test with consideration of the various design variables (Kim *et al*. 2017a).

The design variables of the Y-type perfobond rib include the concrete compressive strength, rib thickness, rib height, rib width, and transverse-rebar diameter. Among the various design variables, the compressive strength of the concrete, transverse rebar, and rib thickness were chosen as the variables to conduct the push-out test for the first time (Kim *et al*. 2013). Thereafter, another push-out test (Kim *et al*. 2014b) was conducted with certain variables, including the rib height and rib width. Another test (Kim *et al*. 2015) was conducted with variables such as the concrete compressive strength and rib thickness. A third set of tests (Kim *et al*. 2017a) was conducted with specific variables, including the rib width, rib height, and transverse-rebar diameter. Table 1 presents the variable conditions used in the previously conducted typical push-out tests (Kim *et al*. 2013, 2014b, 2015, 2017a). Fig. 2 shows the layout and design variables of the specimens. The names of the specimens, given in Table 1, are defined as follows. The specimens are denoted as C30, C40, and C50 when the compressive strengths of the concrete block are 30, 40, and 50 MPa, respectively. They are denoted as T8, T10, and T12 when the rib thicknesses are 8, 10, and 12 mm, respectively. The width and height of the rib are distinguished as W and H, and they were denoted as W60, W80, W100, W120, H80, H100, and H120 based on the dimensions used. The diameter of the transverse rebar is denoted as D. In the case in which the rebar is absent, the diameter is denoted as D0. The specimens with diameters of 13, 16, and 19 mm are denoted as D13, D16, and D19, respectively.

3. Finite element model

3.1 Analysis method

To solve complex problems, such as the nonlinear material property, geometric shape, and contact condition—while performing FEA of the push-out test on the Y-type perfobond rib shear connectors using a static or implicit method—a considerable amount of computational cost is incurred to combine the constitutive, equilibrium, and compatibility equations. To solve these problems, an explicit analysis method has been widely used for complex fracture and large deformation problems under different contact conditions and different material types (Abaqus 2012).

A quasi-static analysis was performed using a dynamic explicit method in FEA of the push-out test on shear connectors (Qureshi *et al*. 2011a, b, Tahmasebinia *et al*. 2013). The analysis time could be reduced by adjusting the material density, loading rate, and time increment in the quasi-static analysis using the dynamic explicit method. In particular, increasing the density could not only reduce the calculation cost, but it also prevented errors due to the wave speed. However, with an increase in the mass density, the dynamic effect that occurs during the calculation also increases. In the quasi-static analysis, which should not be significantly affected by the dynamic effect, the energy balance should be verified to obtain a kinetic energy (KE) that is less than 10% of the internal energy (IE) in the FEA (Abaqus 2012).

3.2 Finite element geometry and mesh

As shown in Fig. 3, the parts in the FEA model for the push-out specimen of the Y-type perfobond rib comprises a steel beam with Y-shaped ribs, transverse rebar, concrete block, reinforcement rebar, and basement. The basement is in contact with the bottom of the specimen. The reinforced rebar is used to prevent the outer fracture of the concrete where the effect of the shear connection is nonexistent. The reinforcement rebar— the influence of which is relatively negligible on the test result—was modeled using a two-

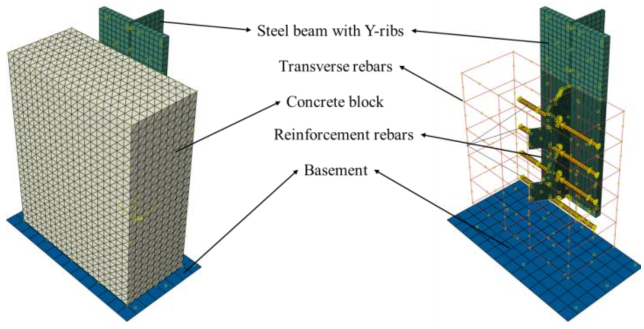

Fig. 3 FEA model of the parts comprising the Y-type perfobond rib

dimensional (2D) beam element, and the basement was prevented from deforming using a four-node rigid element.

For the other parts, except for the reinforcement rebar and basement, a three-dimensional (3D) solid element was employed. Because the shape of the concrete block, excluding that occupied by the cut ribs, was complex, a four-node solid element was employed. The four-node solid element is more effective in preventing errors due to the distortion in the element shape compared to an eight-node solid element. The transverse rebar was modeled as a cylindrical shape with consideration of a nominal cross-sectional area using a six-node wedge solid element, which is suitable for long cylindrical shapes. For the H-beam with the Y-shaped ribs, an eight-node solid element was used.

3.3 Boundary conditions and interactions

The push-out specimen was manufactured to be symmetrical at the flange center of the steel beam about the axis of symmetry, as shown in Fig. 3. Using the specimen symmetry, only half of the specimen was modeled and a symmetric boundary condition was applied. The rigid basement was restricted to move or rotate with respect to any direction, and the displacement occurred at the cross-section of the H-beam in the upper end to apply a similar condition as that in the push-out test. The loading rate was set to 10 mm/s to reduce the analysis time.

The reinforcement comprising the beam element was restrained from the solid element comprising the concrete block using a function of the embedded region using Abaqus. The transverse rebar was rigidly fixed to the concrete contact surface without any separation using a tie function. A frictionless-contact condition was applied to the contact surface between the steel beam with the Y-rib and the concrete block by coating grease (Kim *et al*. 2013, 2014b, 2015, 2017a) while manufacturing the specimen. A lateral separation occurred at the flange of the H-beam and concrete block, which were partly restrained by the frictional force on the bottom surface. Because the frictional resistance between the specimen and the bottom surface in the push-out test affected the test result, an appropriate constraint should be considered for the bottom surface in the FEA.

Generally, a method that considers the friction coefficient between the bottom surface of the concrete block and the basement surface has been employed (Nguyen and Kim 2009, Xu *et al*. 2012). The friction coefficient is in the range of 0.2–0.4. Apart from the above method, another method has been employed to model the separation resistance using the lateral load (Xu *et al*. 2012) and elastic link (Pavlović *et al*. 2013). In the present study, the FEA was conducted with friction coefficients of 0.2, 0.25, 0.3, and 0.4, where 0.25 was chosen as the friction coefficient and yielded a result similar to the existing test results.

3.4 Material models

3.4.1 Concrete

The concrete damaged plasticity (CDP) model was used as the material model of the concrete block. This model can be used to represent the material damage through the decrease in Young's modulus based on the loading level and material characteristics of the concrete. The model also expresses other behaviors depending on whether the nature of loading is compressive or tensile. Hence, it has been widely used in numerical analysis. Because the property of the concrete significantly affects the FEA result of the push-out test, it is necessary to select the stress–strain relationship of the concrete that matches the analysis condition to obtain a practical result. Thus, a compressive softening model of the concrete was selected with consideration of the diameter of the transverse rebar, which significantly affected the concrete behavior.

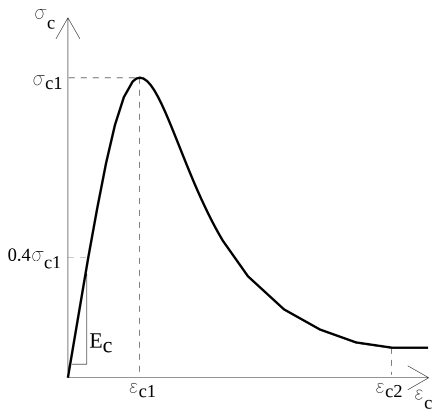

(a) Compressive behavior

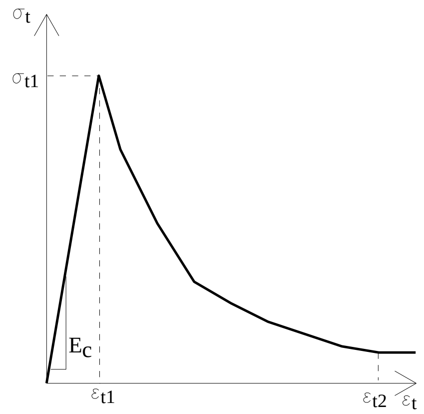

(b) Tensile behavior

Fig. 4 Stress–strain relationship of concrete

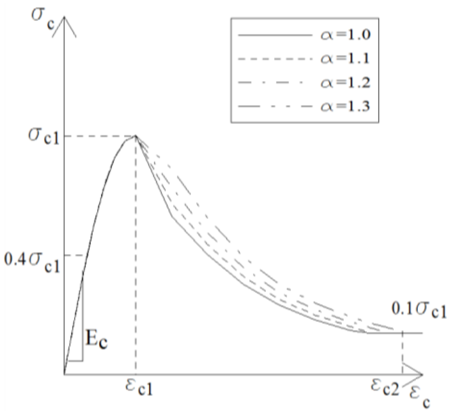

Fig. 5 Variation of compressive curve by α

Fig. 4 shows the stress–strain relationship of the concrete used in this study. The compressive behavior, depicted in Fig. 4(a), is divided into four sections. The first section refers to a region wherein the compressive stress (σ_c) of the concrete is increased up to 0.4 times of the compressive strength (σ_{c1}) in proportion to Young's modulus (E_c), which is the same as the proportional section suggested in Eurocode-2 (BSI 2004). The second section refers to a region wherein σ_c of the concrete reaches from $0.4\sigma_{c1}$ to σ_{c1} (compressive strain: ε_{c1}), which follows the constitutive equation proposed by Mander *et al*. (1998). The third section refers to a region wherein the compressive softening occurs after σ_{c1}. Thus, the compressive stress decreases to $0.1\sigma_{c1}$ at ε_{c2}, which is modified to determine the stress–strain relationship. To this end, a compressive softening coefficient (α) is introduced to correct the effect due to the transverse-rebar diameter in the constitutive equation proposed by Mander *et al*. (1998). Both σ_{c1} and $0.1\sigma_{c1}$ corresponding to ε_{c1} and ε_{c2} respectively are fixed so as not to be affected by α, but the softening behavior between ε_{c1} and ε_{c2} can be influenced by α. Fig. 5 represents the compressive curve according to α. It can be seen that the greater the value of α, the greater the compressive stress in the compressive curve. It is assumed that the compressive stress is maintained as constant after ε_{c2} as the compressive stress is decreased to $0.1\sigma_{c1}$. The compressive stress–strain relationship of the concrete used in this study is expressed in Eqs. (1)-(3).

$$\sigma_c = \varepsilon_c E_c \quad \text{for} \quad 0 < \varepsilon_c \le \frac{0.4\sigma_{c1}}{E_c} \tag{1}$$

where

$\sigma_c =$ Concrete compressive stress (MPa)
$\varepsilon_c =$ Concrete compressive strain
$E_c = 5{,}000\sqrt{\sigma_{c1}}$, concrete tensile stress (MPa)
$\sigma_{c1} =$ Concrete compressive strength (MPa)

$$\sigma_c = \frac{\sigma_{c1} x r}{r - 1 + x^r} \quad \text{for} \quad \frac{0.4\sigma_{c1}}{E_c} < \varepsilon_c \le \varepsilon_{c2} \tag{2}$$

where

$$x = \begin{cases} \dfrac{\varepsilon_c}{\varepsilon_{c1}} & \text{for} \quad \dfrac{0.4\sigma_{c1}}{E_c} < \varepsilon_c \le \varepsilon_{c1} \\ \dfrac{\varepsilon_c}{\varepsilon_{c1}\alpha} & \text{for} \quad \varepsilon_{c1} < \varepsilon_c \le \varepsilon_{c2} \end{cases}$$

ε_{c1} = 0.002, concrete compressive strain at the compressive strength
α = Compressive softening coefficient

$$\boldsymbol{r = \frac{E_c}{E_c - {\sigma_{c1}}/{\varepsilon_{c1}}}}$$

$$\sigma_c = 0.1\sigma_{c1} \quad \text{for} \quad \varepsilon_{c2} < \varepsilon_c \tag{3}$$

The tensile behavior of the concrete is divided into a linear-increase section, stress-decrease section, and stress-maintaining section. The tensile strength (σ_{t1}) is 0.1 times σ_{c1} as per ACI 318 (ACI Committee 1999), and the tensile stress (σ_t) is increased up to σ_{t1} in proportion to E_c, followed by a decrease based on the equation proposed by Wang and Hsu (2001). It is assumed that the tensile stress is maintained to be similar to that of the compressive behavior because σ_t is decreased to $0.1\sigma_{t1}$. The tensile stress–strain relationship of the concrete used in this study is expressed in Eqs. (4)–(6). From Eq. (7) (Pavlović *et al*. 2013), it is assumed that the compressive damage parameter (d_c) and tensile damage parameter (d_t), representing the decrease in the stiffness of the damaged concrete, are expressed via the reduction rate with regard to E_c, which occurs after compressive strength (σ_{c1}) and tensile strength (σ_{t1}).

$$\sigma_t = \varepsilon_t E_c \quad \text{for} \quad 0 < \varepsilon_t \le \varepsilon_{t1} \tag{4}$$

where

$\sigma_t =$ Concrete tensile stress (MPa)
$\varepsilon_t =$ Concrete tensile strain
$\boldsymbol{\varepsilon_{t1}} = \frac{\boldsymbol{\sigma_{t1}}}{\boldsymbol{E_c}}$, concrete tensile strain at the tensile strength
$\sigma_{t1} = 0.1\sigma_{c1}$, concrete tensile strength (MPa)

$$\sigma_t = \sigma_{t1}\left(\frac{\varepsilon_{t1}}{\varepsilon_t}\right)^{0.4} \quad \text{for} \quad \varepsilon_{t1} < \varepsilon_t \le \varepsilon_{t2} \tag{5}$$

$$\sigma_t = 0.1\sigma_t \quad \text{for} \quad \varepsilon_{t2} < \varepsilon_t \tag{6}$$

$$\begin{aligned} d_c &= 1 - \frac{\sigma_c}{\sigma_{c1}} \quad for \quad \varepsilon_{c1} < \varepsilon_c \\ d_t &= 1 - \frac{\sigma_t}{\sigma_{t1}} \quad for \quad \varepsilon_{t1} < \varepsilon_t \end{aligned} \tag{7}$$

where

d_c = Compressive damage parameter
d_t = Tensile damage parameter

3.4.2 Structural steel and reinforcement

The structural steel and reinforcement were modeled using an isotropic hardening material, Poisson's ratio, was set to 0.3, and Young's modulus, which was set to 210 GPa and 200 GPa. Figs. 6(a) and (b) show the stress–strain relationships of the structural steel and reinforcement used

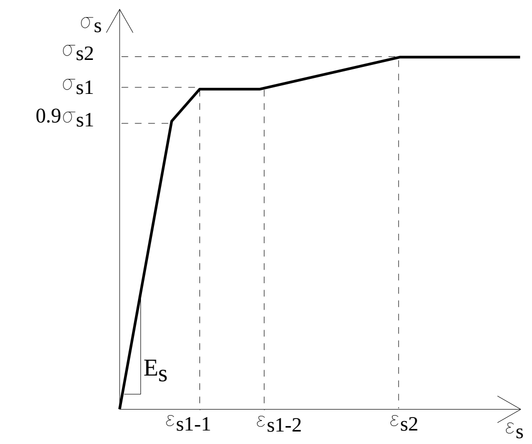

(a) Structural steel

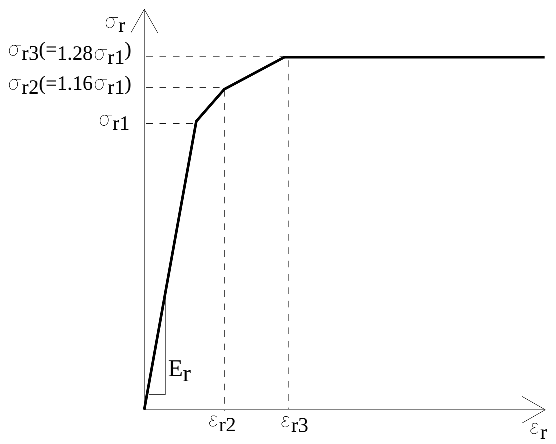

(b) Reinforcement

Fig. 6 Stress–strain relationships of structural steel and reinforcement

in the FEA (Veritas 2013, Loh *et al*. 2004), respectively. The parameters that define the stress–strain relationship of the materials were employed considering the material properties used in the test as follows: σ_{s1}: 300 MPa, σ_{s2}: 450 MPa, ε_{s1-1}: 0.004, ε_{s1-2}: 0.02, ε_{s2}: 0.2, σ_{r1}: 500 MPa, ε_{r2}: 0.0225, and ε_{r3}: 0.1.

4. Verification of the finite element model

Studies on the variables, including the concrete compressive strength (C30/C40/C50), rib thickness (T8/T10/T12), rib width (W60/W80/W100/W120), rib height (H80/H100/H120), and transverse-rebar diameter (D13/D16/D19), were conducted based on the criteria of C40-T10-W80-H100-D16, as given in Table 1. The concrete compressive strength, rib thickness, rib width, rib height, and transverse-rebar diameter were 40 MPa, 10 mm, 80 mm, 100 mm, and 16 mm, respectively, in the tests conducted on Y-type perfobond shear connectors to date (Kim *et al*. 2013, 2014b, 2015, 2017a). Because it is very difficult to measure the frictional force generated at the bottom surface during the push-out test, a suitable friction coefficient (0.2–0.4) that yields a similar result as that of the experiment result was selected and used in the FEA of the

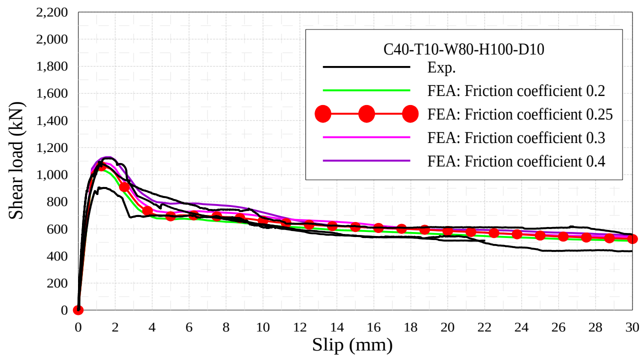

Fig. 7 Effect of friction coefficient on load–slip curve

push-out test (Nguyen and Kim 2009, Xu *et al*. 2012). Friction coefficients of 0.2, 0.25, 0.3, and 0.4 were applied to the variable conditions (C40-T10-W80-H100-D0) in the case of no transverse rebar to perform the FEA. The load–slip curve was compared with the experimental results, as shown in Fig. 7. An increasing trend in the relative slip where the shear strength occurred and the magnitude of the shear strength with an increase in the friction coefficient was revealed. In the present study, the friction coefficient was 0.25, which yielded a result notably similar to the test result.

The mass density of the material significantly affected the computational cost in the quasi-static analysis using the dynamic explicit method. A mass scale technique could be used to reduce the time consumption in the FEA, including complex contact nonlinearity, material nonlinearity, and geometric nonlinearity, which were the same as those in the push-out test on the Y-type perfobond rib shear connectors (Abaqus 2012). Although an increase in the mass density could reduce the analysis time and occurrence probability of the numerical error due to the wave speed, a post procedure should be used to correct the dynamic effect. In the post-procedure, the dynamic effect is eliminated by incorporating a smooth function using Abaqus (2012).

The FEA was conducted by applying the same time increment and loading rate to compare and analyze the mass-density effect. The time required to generate a relative displacement of 1 mm based on the mass density is summarized as follows based on the analysis time that was actually used in the material-property mass density. Based on the analysis time applied to the actual mass density, the analysis time decreased by 66.2, 90.5, and 97.5% in the cases wherein the mass density was increased by 10, 100, and 1,000 times, respectively. In this study, a mass density 1,000 times that of the original was used with consideration of the energy balance satisfying the quasi-static analysis condition and the time required for the FEA. The results with and without the post procedure applied to the load–slip curve of C40-T10-W80-H100-D16, which was obtained in the FEA, were compared with the test results, as shown in Fig. 8(a). The blue in that figure indicates the dynamic effect at the early stage of the loading, whereas the red line indicates the results closer to the static condition through the post-procedure. Fig. 8(b) shows the kinetic energy (KE) and internal energy (IE) during the quasi-static analysis in the log scale. Although the dynamic effect significantly

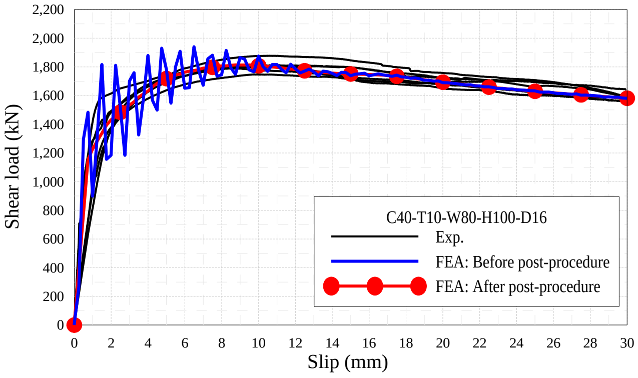

(a) Load–slip curve

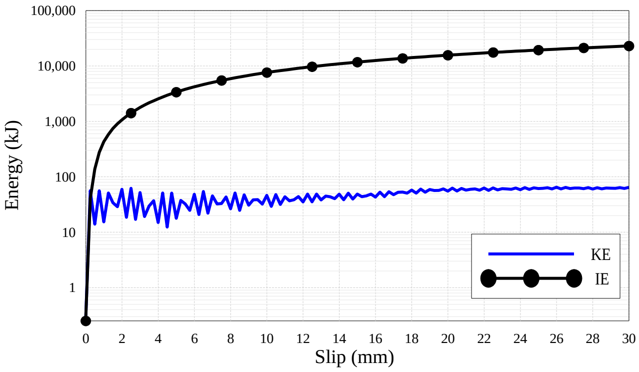

(b) Energy history

Fig. 8 Load–slip curve to which post-procedure is applied and energy history generated in the FEA

occurred in the FEA at the early stages of loading, quasi-static analysis was considered to be appropriate because the generation of KE was considerably lower than that of IE, as shown in Fig. 8(b).

4.1 Effect of transverse rebar

The transverse rebars in the Y-type perfobond and flat-type perfobond rib shear connectors help ensure the shear strength and ductile behavior. The transverse rebars in the Y-type perfobond shear connectors generate complex bending and shear stresses because of the surrounding concrete along with the ribs. Thus, it is necessary to develop a constitutive equation wherein the effect of the transverse rebar is reflected in the stress–strain relationship considering the confined effect of the general concrete (Mander *et al.* 1988). Accordingly, α of the compressive behavior in Eq. (3) was adjusted based on the effect of the transverse-rebar diameter to determine the compressive softening.

Figs. 9(a), (b), and (c) show the FEA of D13, D16, and D19, respectively, when α equals 1.0, 1.1, 1.2, and 1.3. For C40-T10-W80-H100-D13, the FEA is 1634, 1659, 1696, and 1716 kN, respectively, when α equals 1.0, 1.1, 1.2, and 1.3 and the mean shear strength in the test result is 1540 kN. For C40-T10-W80-H100-D16, the result of the FEA is 1781, 1814, 1822, and 1884 kN when α equals 1.0, 1.1, 1.2, and 1.3, respectively. The mean shear strength is 1805 kN. For C40-T10-W80-H100-D19, the FEA is 1912, 1949,

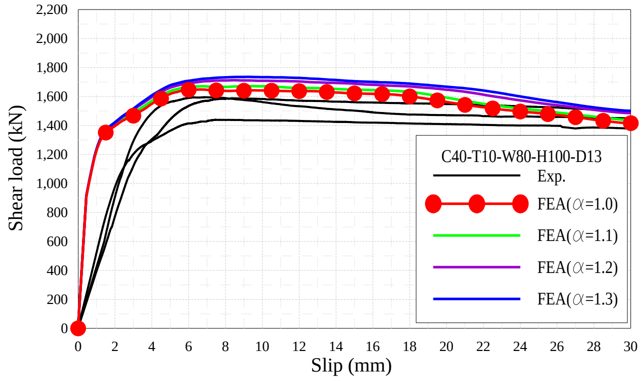

(a) Transverse rebar D13

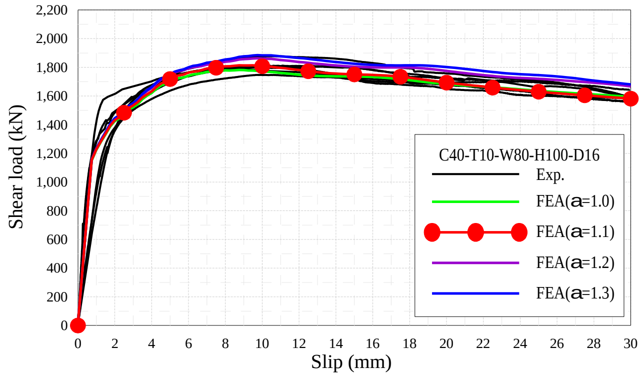

(b) Transverse rebar D16

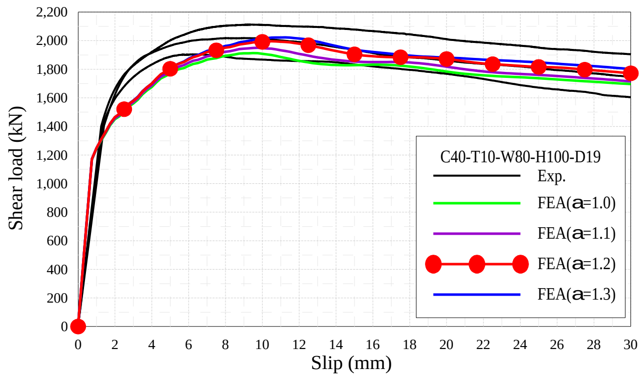

(c) Transverse rebar D19

Fig. 9 Comparison of load–slip curve between test results and FEA with respect to the transverse-rebar diameter

1995, and 2022 kN, respectively, when α equals 1.0, 1.1, 1.2, and 1, and the mean shear strength in the test result is 2011 kN. As α increases, the shear strength increases. The most similar shear strength is found when α is 1.0 for D13 of the transverse-rebar diameter; α is 1.1 for D16, and α is 1.2 for D19.

4.2 Effect of concrete strength

Fig. 10 shows the specimen load–slip curve of the based on the concrete compressive strength. As the concrete compressive strength increases from C30 to C40 and C50, the shear strength of the specimen increases. This trend is also revealed in the FEA result. Table 2 presents the test and

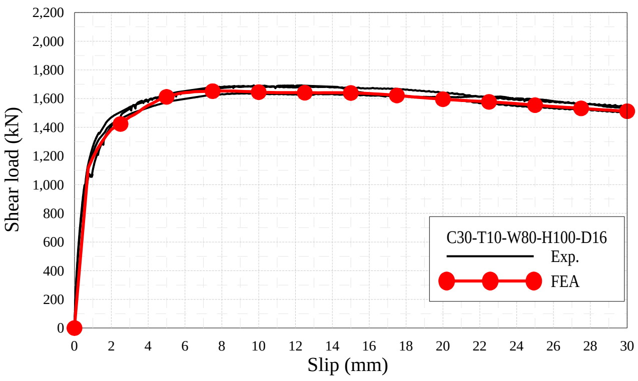

(a) 30 MPa

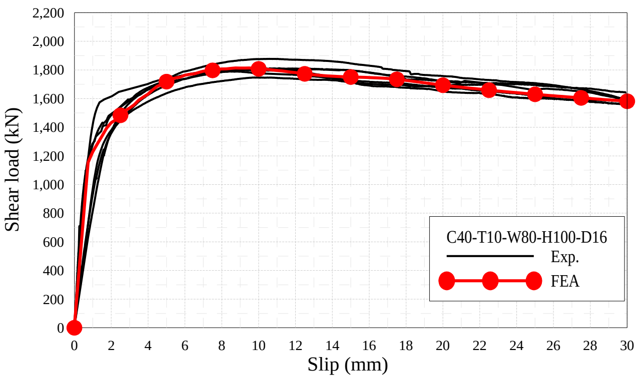

(b) 40 MPa

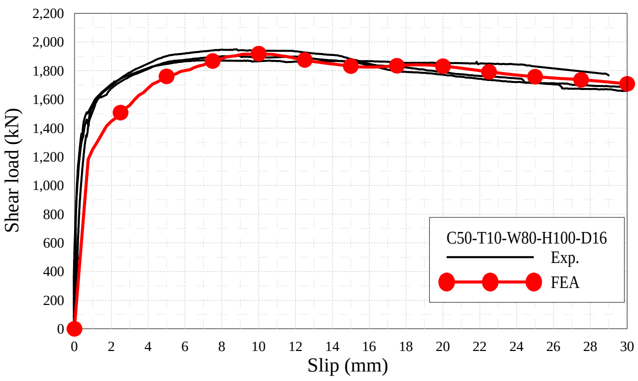

(c) 50 MPa

Fig. 10 Comparison of load–slip curves between test results and FEA with respect to the compressive strength of concrete

Table 2 Comparison of shear strengths between test results and FEA with respect to the compressive strength of concrete

		Shear strength (kN)	COV (%)
C30-T10-W80-H100-D16*	Exp.-1	1687	0.93
	Exp.-2	1638	2.10
	Exp.-3	1691	1.16
	Average	1672	-
	FEA	1652	Error: −1.17%
C40-T10-W80-H100-D16*	Exp.-1	1811	0.31
	Exp.-2	1789	0.91
	Exp.-3	1810	0.24
	Exp.-4	1877	3.98
	Exp.-5	1,747	3.25
	Exp.-6	1799	0.38
	Average	1805	-
	FEA	1813	Error: 0.44%
C50-T10-W80-H100-D16*	Exp.-1	1949	2.14%
	Exp.-2	1872	1.89%
	Exp.-3	1903	0.25%
	Average	1908	-
	FEA	1919	Error: 0.55%

*Specimen with eight ribs

FEA results. The coefficients of variation (COV) of the test results in C30-T10-W80-H100-D16, C40-T10-W80-H100-D16, and C50-T10-W80-H100-D16 are within 4%, and the error in the FEA is within 1.2%. Thus, the above results verified that the FEA results obtained in this study reflected an increase in the shear strength based on the increase in the compressive strength of the concrete.

4.3 Effect of rib dimension

Figs. 11 to 13 and Tables 3 to 5 present the test and FEA results with respect to different rib thicknesses, rib heights, and rib widths. The shear strength of the specimen increases as the thickness, height, and width of the rib increases,

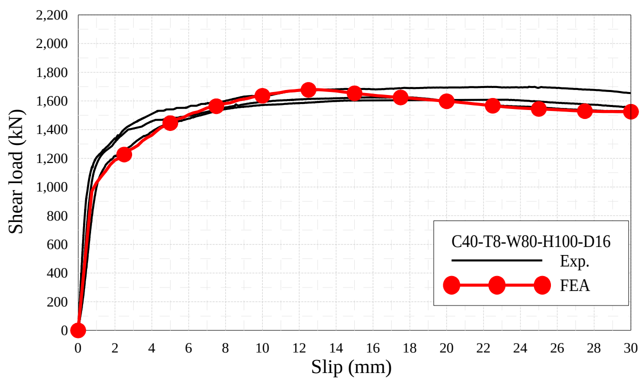

(a) 8 mm

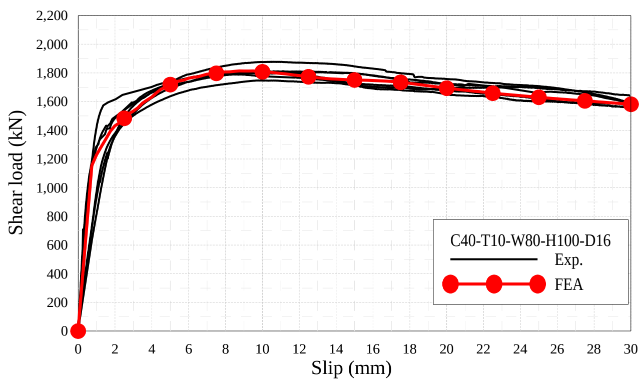

(b) 10 mm

Fig. 11 Comparison of load–slip curve between test results and FEA with respect to the rib thickness

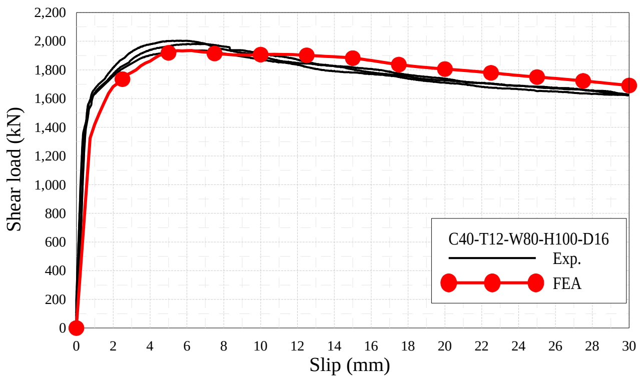

(c) 12 mm

Fig. 11 Continued

Table 3 Comparison of shear strength between test results and FEA with respect to the rib thickness

		Shear strength (kN)	COV (%)
C40-T8-W80-H100-D16*	Exp.-1	1699	3.23
	Exp.-2	1630	0.92
	Exp.-3	1608	2.31
	Average	1646	-
	FEA	1678	Error: 1.97%
C40-T10-W80-H100-D16*	Exp.-1	1811	0.31
	Exp.-2	1789	0.91
	Exp.-3	1810	0.24
	Exp.-4	1877	3.98
	Exp.-5	1747	3.25
	Exp.-6	1799	0.38
	Average	1805	-
	FEA	1813	Error: 0.44%
C40-T12-W80-H100-D16*	Exp.-1	2003	1.53
	Exp.-2	1935	1.91
	Exp.-3	1980	0.38
	Average	1973	-
	FEA	1934	Error: −1.96%

*Specimen with eight ribs

which is the same as those observed for the diameter of the transverse rebar and compressive strength of the concrete. The COVs of the shear strength based on the test results are all within 4.5%, and the shear strength with respect to the rib thickness exhibits an error within 2% between the FEA and test results. However, the shear strength with respect to the height and width of the rib exhibits an error up to 9.5% and 12.6%, respectively, which are higher than that of the overall test result. This is because the more accurate properties of the materials used in the tests with variables, such as the height and width of the rib (specimens with four ribs), were not applied in the FEA, wherein only the variables, such as the diameter of the transverse rebar and concrete compressive strength (specimens with eight ribs), were employed.

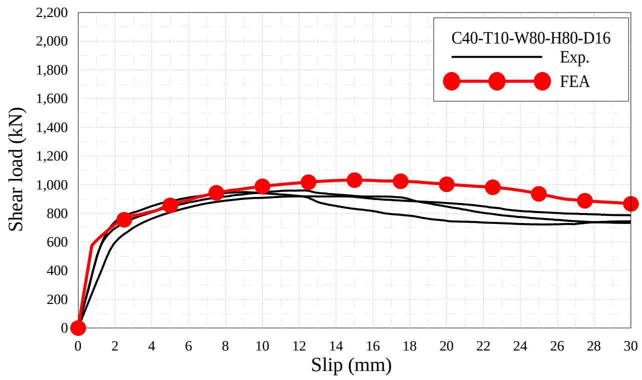

(a) 80 mm

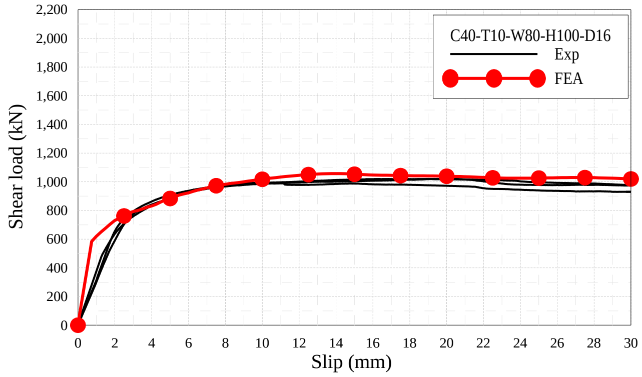

(b) 100 mm

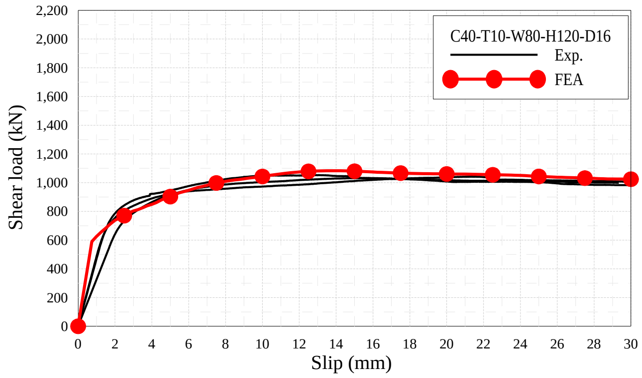

(c) 120 mm

Fig. 12 Comparison of load–slip curves between test results and FEA with respect to the rib height

5. Shear strength equation for stubby Y-type perfobond rib shear connection

The stubby Y-type perfobond rib shear connector is smaller than the conventional Y-type perfobond rib shear connector. This type of shear connector was studied by Kim *et al*. (2017b), who performed monotonic push-out tests. Based on the details of the stubby Y-type perfobond rib shear connector in Fig. 14, the finite element analysis model was built in the same way that was mentioned above. The variable was set to the diameter of the transverse rebar, and the diameters were applied to 10 mm, 13 mm, and 16 mm.

The SY, D, and M denotes the stubby Y-type perfobond rib shear connector, the diameters of the transverse rebar, and monotonic force, respectively.

Table 4 Comparison of shear strength between test results and FEA with respect to the rib height

		Shear strength (kN)	COV (%)
C40-T10-W80-H80-D16**	Exp.-1	948	0.62
	Exp.-2	959	1.85
	Exp.-3	919	2.47
	Average	942	-
	FEA	1031	Error: 9.50%
C40-T10-W80-H100-D16**	Exp.-1	992	1.85
	Exp.-2	1019	0.83
	Exp.-3	1021	1.02
	Average	1010	-
	FEA	1057	Error: 4.56%
C40-T10-W80-H120-D16**	Exp.-1	1153	3.02
	Exp.-2	1087	2.86
	Exp.-3	1118	0.15
	Average	1119	-
	FEA	1188	Error: 6.13%

*Specimen with four ribs

The load–slip curves are shown in Fig. 15, which presents the experimental data and FEA data. The ultimate shear resistance is fully expected by the FEA model in the comparison of the experimental data. However, after the ultimate shear resistance, there is a limit to expecting the behavior of the stubby Y-type perfobond rib shear connector with the FEA model.

The previous shear resistance equation suggested by Kim *et al*. (2015) is the same as Eq. (8). It is based on the push-out test results of the conventional Y-type perfobond rib shear connector. In order to confirm the effectiveness of the equation for the stubby Y-type perfobond rib shear connector, the test results of the specimen of SY-D10-M, SY-D13-M, and SY-D16-M were used in a comparison with the predicted shear resistance calculated from Eq. (8), where Q (N) represents the shear resistance of the Y-type perfobond rib shear connector, d (mm) is the dowel hole diameter, h (mm) is the individual rib height, t (mm) denotes the rib thickness, f_{ck} (MPa) represents the concrete strength, d_t (mm) is the transverse rebar diameter, and A_{tr} (mm^2) is the cross sectional area of the transverse rebar. In addition, f_y (MPa) denotes the transverse rebar's yield strength, r is the number of transverse rebars, n denotes the number of holes between the ribs, m is the number of dowel areas between Y-shape ribs, and s (mm) represents the net distance between ribs that are bent in the same direction. The comparison results are listed in Table 6. It is apparent that a difference exists

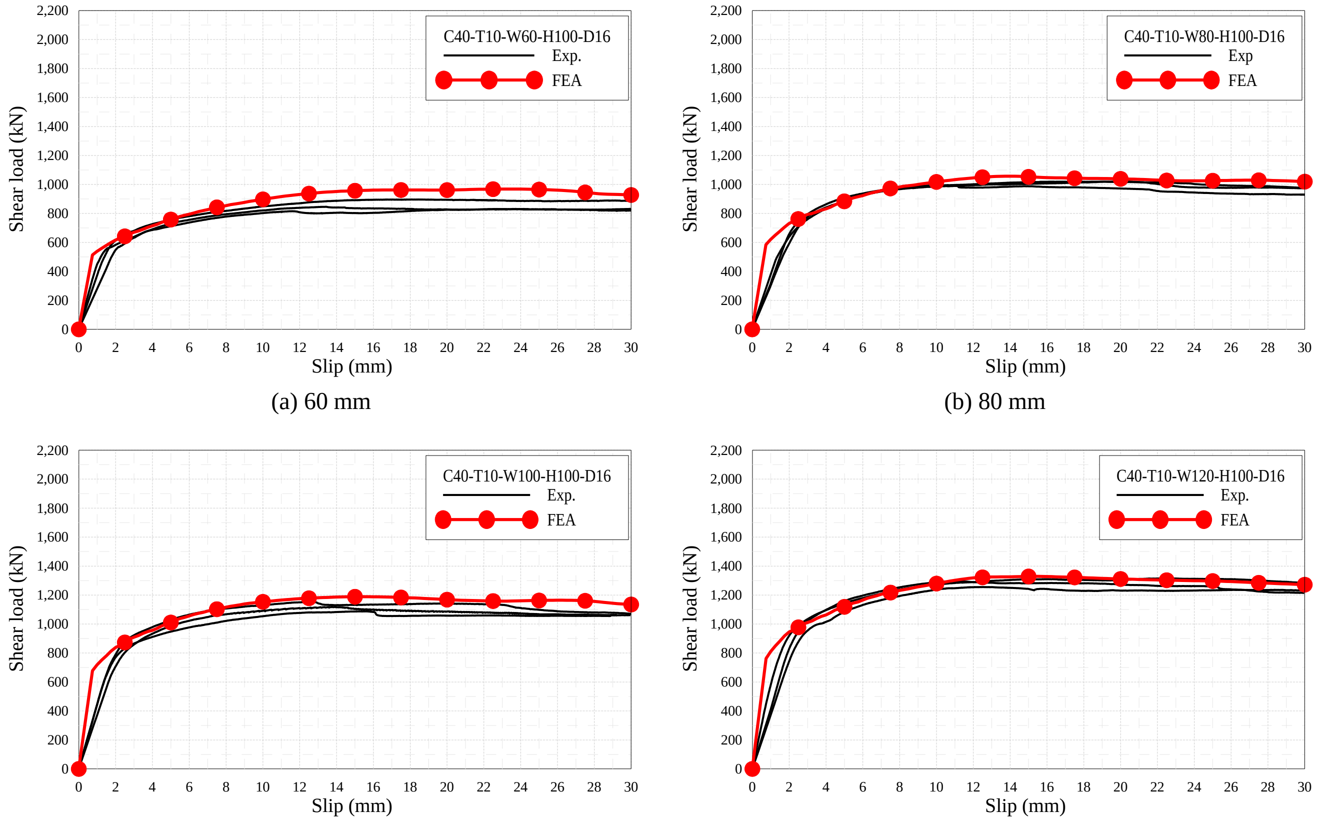

(a) 60 mm

(b) 80 mm

(c) 100 mm

(d) 120 mm

Fig. 13 Comparison of load–slip curve between the test results and FEA with respect to the rib width

Table 5 Comparison of shear strength between test results and FEA with respect to the rib width

		Shear strength (kN)	COV (%)
C40-T10-W60-H100-D16**	Exp.-1	896	4.21
	Exp.-2	845	1.68
	Exp.-3	838	2.53
	Average	860	-
	FEA	968	Error: 12.57%
C40-T10-W80-H100-D16**	Exp.-1	992	1.85
	Exp.-2	1019	0.83
	Exp.-3	1021	1.02
	Average	1010	-
	FEA	1057	Error: 4.56%
C40-T10-W100-H100-D16**	Exp.-1	1153	3.34
	Exp.-2	1087	3.17
	Exp.-3	1118	0.17
	Average	1119	-
	FEA	1188	Error: 6.13%
C40-T10-W120-H100-D16**	Exp.-1	1315	2.06
	Exp.-2	1255	2.58
	Exp.-3	1295	0.52
	Average	1288	-
	FEA	1328	Error: 3.12%

*Specimen with four ribs

the experimental results and calculated results using Eq. (8). The shear resistances of the experiment for the stubby Y-type perfobond rib shear connector are much different than that of the calculation using Eq. (8), because Eq. (8) is based on the conventional Y-type perfobond rib shear connector. In the previous study by Kim *et al*. (2017b), it was found that the equation had a limitation in evaluating the ultimate shear resistance of the stubby Y-type perfobond rib shear connector. Moreover, the limiting factor governing the prediction of the effect of the transverse rebar diameter was also found. As a result, in the case of the stubby Y-type perfobond rib shear connector, the results of Eq. (8) are considerably different from the experiment results. Kim *et al*. (2017b) performed the push-out test and represented the difference between the results of the experiment and evaluation using Eq. (8) considering the transverse rebar variable. According to the results of the experiment, the specimen with the smaller diameter had lower shear strength compared to the evaluation using Eq. (8). On the other hand, the specimen with the greater diameter showed higher shear strength compared to the evaluation using Eq. (8). Thus, Eq. (8) either under-estimated or overestimated the value. Thus, in order to develop the equation for the stubby Y-type perfobond rib shear connector and consider the effect of the diameters of the transverse rebar, the factor term for the transverse rebar is modified with the previous equation (Eq. (8)). The proposed equation is Eq. (9), which is modified to the factor in the transverse rebar term with the quadratic function depending on the diameter of transverse rebar (d_t) resulted by a regression analysis.

Table 6 shows the results of shear resistance by the experiments and the proposed equation (Eq. (9)). The specimens for the experiment are manufactured with concrete strength 30 MPa and yield strength of the transverse rebar 400 MPa, and the dimension of the specimens is followed in Fig. 14. The accuracy of the proposed equation (Eq. (9)) is approximately 97% on average, while that of the previous equation (Eq. (8)) is approximately 73% on average. It can be observed that the propose equation (Eq. (9)) is under 3% error, and more

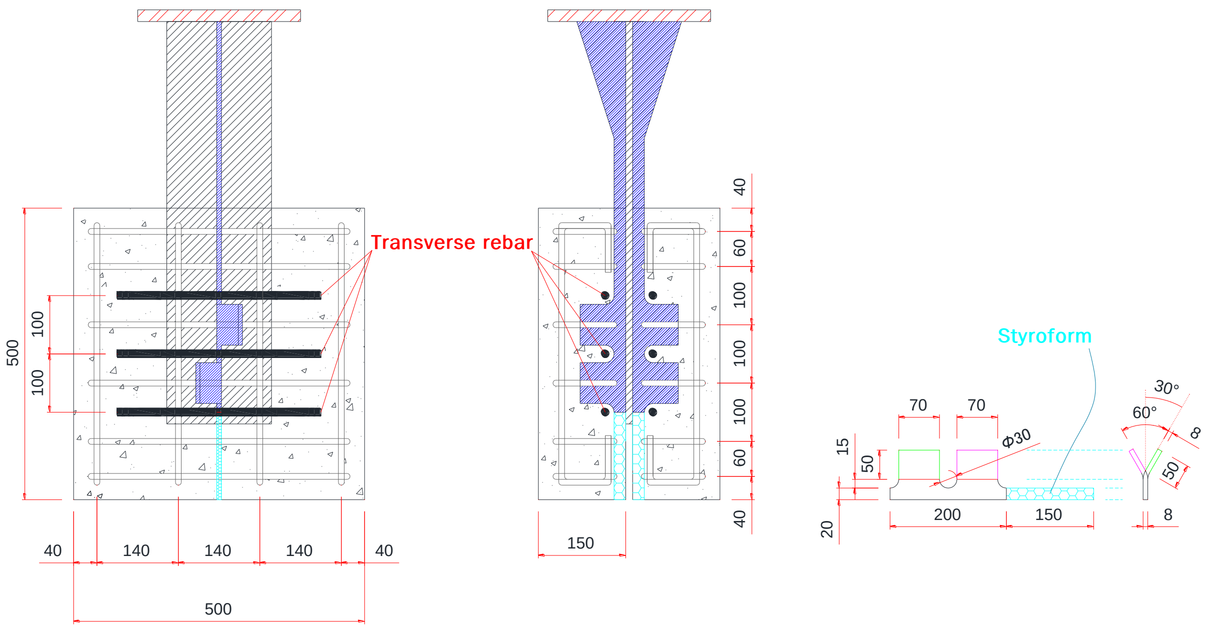

(a) Front view (b) Side view (c) Details of stubby Y-rib

Fig. 14 Details of the specimen of the stubby Y-type perfobond rib shear connector (unit: mm) accurate to estimate the shear resistance for the stubby Y-type perfobond rib shear connector.

The parametric studies were performed depending on the variables of the concrete compressive strength and transverse rebar diameter with Eq. (9) and FEA models. The kinds of concrete compressive strengths were set to 20 MPa, 25 MPa, 30 MPa, 35 MPa, 40 MPa, 45 MPa, and 50 MPa, and those of the transverse rebar (f_y = 400 MPa) were set to 10 mm, 13 mm, and 16 mm.

Table 7 and Fig. 16 represent the comparison of the predicted (Eq. (9)) and FEA results. On Table 7, it can be observed that the margin of error calculated using Eq. (9) is under 7%. The margin of error using the quadratic function for the factor is much smaller than that of the previous factor 1.213 from Eq. (8). Therefore, the proposed equation not only more accurately estimates the shear resistance of the stubby Y-type perfobond rib shear connection.

$$Q = 3.372\left(\frac{d}{2}+2h\right)tf_{ck} + 1.213rA_{tr}f_y \\ +1.9n\pi\left(\frac{d}{2}\right)^2\sqrt{f_{ck}} + 0.757mhs\sqrt{f_{ck}} \tag{8}$$

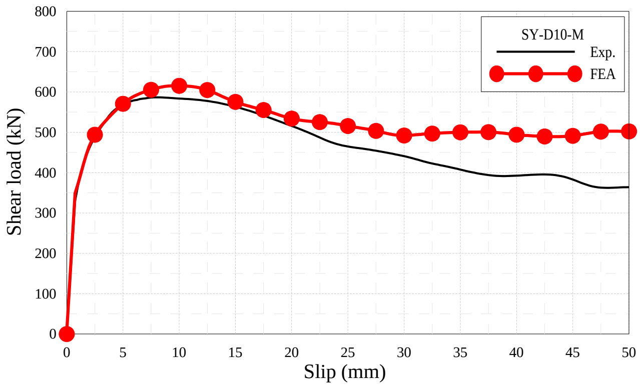

(a) SY-D10-M

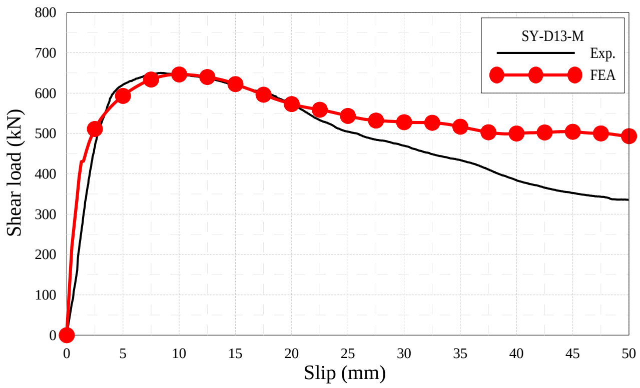

(b) SY-D13-M

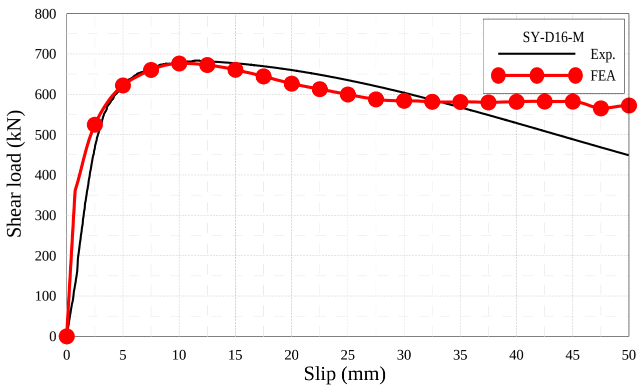

(c) SY-D16-M

Fig. 15 Results of the stubby Y-type perfobond rib shear connector with FEA

Table 7 Verification of the suggested equation (Eq. (9)), and the results of parametric studies

Division	Specimen	Shear resistance (kN)		Ratio (A)/(B)
		FEA (A)	Eq. (9) (B)	
C20	SY-D10-M	524.2	488.7	1.07
	SY-D13-M	559.9	561.4	1.00
	SY-D16-M	596.5	592.4	1.01
C25	SY-D10-M	543.9	521.7	1.04
	SY-D13-M	578.7	594.3	0.97
	SY-D16-M	611.3	625.3	0.98
C30	SY-D10-M	615.2	554.5	1.11
	SY-D13-M	646.1	627.1	1.03
	SY-D16-M	676.4	658.1	1.03
C35	SY-D10-M	642.7	587.2	1.09
	SY-D13-M	668.5	659.8	1.01
	SY-D16-M	700.6	690.9	1.01
C40	SY-D10-M	665.7	619.8	1.07
	SY-D13-M	694.6	692.5	1.00
	SY-D16-M	725.6	723.5	1.00
C45	SY-D10-M	676.7	652.4	1.04
	SY-D13-M	708.1	725.1	0.98
	SY-D16-M	736.7	756.1	0.97
C50	SY-D10-M	697.1	684.9	1.02
	SY-D13-M	724.8	757.6	0.96
	SY-D16-M	760.1	788.6	0.96

Table 6 Comparison of the results between measured data and predicted data using Eqs. (8) and (9)

	Shear resistance by experiment (kN) (A)	Shear resistance using Eq. (8) (kN) (B)	Ratio (B)/(A)	Shear resistance using Eq. (9) (kN) (C)	Ratio (C)/(A)
SY-D10-M	586.5	353.3	0.60	554.5	0.95
SY-D13-M	643.8	458.5	0.71	627.1	0.97
SY-D16-M	674.1	591.1	0.88	658.1	0.98

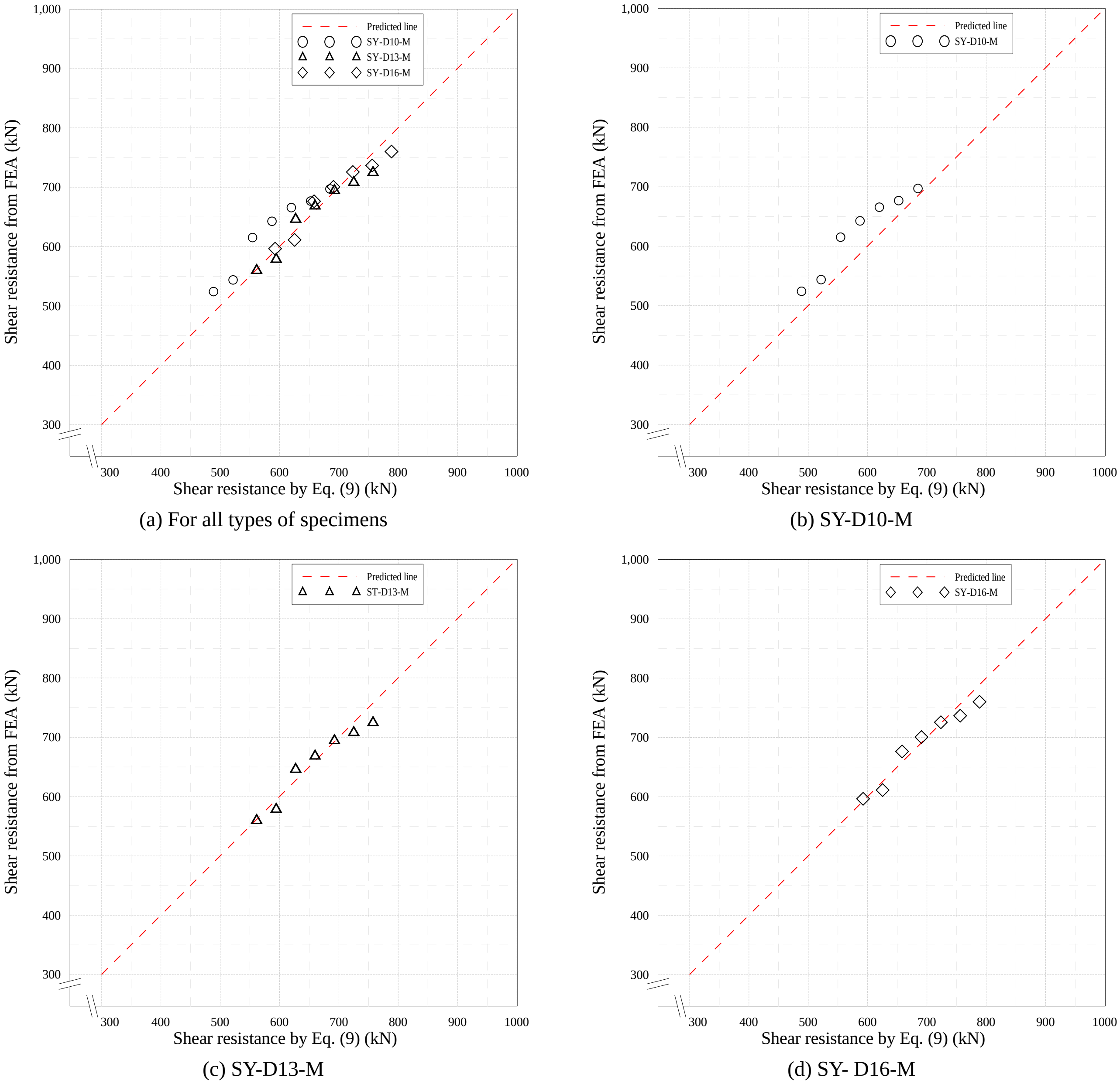

(a) For all types of specimens

(b) SY-D10-M

(c) SY-D13-M

(d) SY- D16-M

Fig. 16 Comparison of the FEA results and predicted results

$$
\begin{aligned}
Q = 3.372\left(\frac{d}{2}+2h\right)tf_{ck} \\
+\left(0.012{d_t}^2-0.5416d_t+7.005\right)rA_{tr}f_y \qquad (9) \\
+1.9n\pi\left(\frac{d}{2}\right)^2\sqrt{f_{ck}}+0.757mhs\sqrt{f_{ck}}
\end{aligned}
$$

6. Conclusions

In this study, numerical simulations on Y-type perfobond rib shear connectors were conducted to compare the load–slip curves of existing test results. The FEM results were similar to those of the previous study using push-out tests. Using the newly developed model, a parametric study was conducted. Based on the results, a new shear resistance formula was suggested. The contributions and conclusions of this study are outlined as follows.

(1) Compared to existing techniques, a more efficient quasi-static analysis technique was proposed by adjusting the mass density of the materials to reduce the analysis time. An increase in the material density increased the dynamic effect of the FEA results. However, the present study verified that, if this problem could be appropriately solved through the post-procedure, satisfactory results could be obtained with a manageable computational cost.

(2) The compressive softening of the stress–strain relationship of the concrete was modified and applied based on the diameter of the transverse rebar. The stress–strain relationship, which was

improved using the compressive softening coefficient α, yielded results similar to the existing test results. The improved material property of the concrete in this study can be appropriately applied to numerical simulations to conduct the push-out test on various shear connectors with a transverse rebar.

(3) An increase in the shear strength was well reflected based on the increases in the thickness, height, and width of the rib. The difference in the shear strength due to the changes in the height and width of the rib—which were variables of the specimens comprising the four ribs—revealed that the FEA results were somewhat higher than the test results. However, the shapes of the load–slip curves were similar. An error in the shear strength was obtained because accurate material properties used in the actual tests were not applied to the FEA.

(4) The FEA for the stubby Y-type perfobond rib shear connector was conducted by the suggested modeling technique. The FEA results were fully expected with respect to the ultimate shear resistance. However, a limitation existed; specifically, it was difficult to reflect the structural behavior after the ultimate shear resistance.

(5) The accurate shear resistance equation for the stubby Y-type perfobond rib shear connector is herein proposed, modifying the equation for the conventional Y-type perfobond rib shear connector suggested by Kim *et al*. (2015). The factor of the transverse rebar has been modified to the quadratic function, which is accurate to calculate the shear resistance for the stubby Y-type perfobond rib shear connector. The parametric study is performed by comparing the results from FEA and the proposed equation. Depending on the variations with concrete strength and the diameter of the transverse rebar, it can be seen that the proposed equation well expected the shear resistance of the stubby Y-type perfobond rib shear connector.

Acknowledgments

This work was supported by the Korea Institute of Energy Technology Evaluation and Planning (KETEP) and the Ministry of Trade, Industry & Energy (MOTIE) of the Republic of Korea (No. 20174030201480). This work was supported by the Korea Institute of Energy Technology Evaluation and Planning (KETEP) and the Ministry of Trade, Industry & Energy(MOTIE) of the Republic of Korea (No. 20181510102410).

References

Abaqus Documentation, Version 6.12 (2012), Dassault System, USA.

ACI Committee (1999), Building code requirements for structural concrete (ACI 318M-99) and Commentary (ACI 318RM-99); American Concrete Institute.

Al-Darzi, S.Y.K., Chen, A.R. and Liu, Y.Q. (2007), "Finite element simulation and parametric studies of perfobond rib connector", *Am. J. Appl. Sci*., **4**(3), 122-127.

British Standards Institution (BSI) (2004), Eurocode 2: Design of Concrete Structures: Part 1-1: General Rules and Rules for Buildings; British Standards Institution.

Classen, M. and Herbrand, M. (2015), "Shear behaviour of composite dowels in transversely cracked concrete", *Struct. Concrete*, **16**(2), 195-206.

Dai, X.H., Lam, D. and Saveri, E. (2015), "Effect of concrete strength and stud collar size to shear capacity of demountable shear connectors", *J. Struct. Eng*., **141**(11), 04015025.

European Committee for Standardization (CEN) (2004), Design of Composite Steel and Concrete Structures, Part 1.1: General Rules and Rules for Buildings, EN1994-1-1; European Committee for Standardization, Brussels, Belgium.

Hechler, O., Berthellemy, J., Lorenc, W., Seidl, G. and Viefhues, E. (2011), "Continuous Shear Connectors in Bridge Construction", In" *Composite Construction in Steel and Concrete VI*, pp. 78-91.

Khorramian, K., Maleki, S., Shariati, M., Jalali, A. and Tahir, M.M. (2017), "Numerical analysis of tilted angle shear connectors in steel-concrete composite systems", *Steel Compos. Struct*., *Int. J*., **23**(1), 67-85.

Kim, S.E. and Nguyen, H.T. (2010), "Finite element modeling and analysis of a hybrid steel–PSC beam connection", *Eng. Struct*., **32**(9), 2557-2569.

Kim, S.H., Choi, K.T., Park, S.J., Park, S.M. and Jung, C.Y. (2013), "Experimental shear resistance evaluation of Y-type perfobond rib shear connector", *J. Constr. Steel Res*., **82**, 1-18.

Kim, S.H., Choi, J., Park, S.J., Ahn, J.H. and Jung, C.Y. (2014a), "Behavior of composite girder with Y-type perfobond rib shear connectors", *J. Constr. Steel Res*., **103**, 275-289.

Kim, S.H., Heo, W.H., Woo, K.S., Jung, C.Y. and Park, S.J. (2014b), "End-bearing resistance of Y-Type perfobond rib according to rib width–height ratio", *J. Constr. Steel Res*., **103**, 101-116.

Kim, S.H., Park, S.J., Heo, W.H. and Jung, C.Y. (2015), "Shear resistance characteristic and ductility of Y-Type Perfobond Rib Shear Connector", *Steel Compos. Struct*., *Int. J*., **18**(2), 497-517.

Kim, S.H., Kim, K.S., Park, S., Ahn, J.H. and Lee, M.K. (2016), "Y-type perfobond rib shear connectors subjected to fatigue loading on highway bridges", *J. Constr. Steel Res*., **122**, 445-454.

Kim, S.H., Park, S., Kim, K.S. and Jung, C.Y. (2017a), "Generalized formulation for shear resistance on Y-type perfobond rib shear connectors", *J. Constr. Steel Res*., **128**, 245-260.

Kim, S.H., Kim, K.S., Lee, D.H., Park, J.S. and Han, O. (2017b), "Analysis of the shear behavior of stubby Y-type perfobond rib shear connectors for a composite frame structure", *Materials*, **10**(11), 1340-1358.

Kim, S.H., Kim, K.S., Park, S., Jung, C.Y. and Choi, J.G. (2017c), "Comparison of hysteretic performance of stubby Y-Type Perfobond rib and stud shear connectors", *Eng. Struct*., **147**, 114-124.

Kim, S.H., Kim, K.S., Han, O. and Park, J.S. (2018a), "Influence of transverse rebar on shear behavior of Y-type perfobond rib shear connection", *Constr. Build. Mater*., **180**, 254-264.

Kim, S.H., Han, O., Kim, K.S. and Park, J.S. (2018b), "Experimental behavior of double-row Y-type perfobond rib shear connectors", *J. Constr. Steel Res*., **150**, 221-229.

Kim, K.S., Han, O., Choi, J. and Kim, S.H. (2019), "Hysteretic performance of stubby Y-type perfobond rib shear connectors depending on transverse rebar", *Constr. Build. Mater*., **200**, 64-79

Leonhardt, F., Andrä, W., Andrä, H.P. and Harre, W. (1987), "New advantageous shear connection for composite structures with high fatigue strength", *Beton-und Stahlbetonbau*, **62**(12), 325-331.

Loh, H.Y., Uy, B. and Bradford, M.A. (2004), "The effects of partial shear connection in the hogging moment regions of composite beams: Part I—Experimental study", *J. Constr. Steel Res.*, **60**(6), 897-919.

Maleki, S. and Bagheri, S. (2008), "Behavior of channel shear connectors, Part II: Analytical study", *J. Constr. Steel Res.*, **64**(12), 1341-1348.

Mander, J.B., Priestley, M.J. and Park, R. (1988), "Theoretical stress-strain model for confined concrete", *Journal of Structural Engineering*, **114**(8), 1804-1826.

Nguyen, H.T. and Kim, S.E. (2009), "Finite element modeling of push-out tests for large stud shear connectors", *J. Constr. Steel Res.*, **65**(10), 1909-1920.

Oguejiofor, E.C. and Hosain, M.U. (1997), "Numerical analysis of push-out specimens with perfobond rib connectors", *Comput. Struct.*, **62**(4), 617-624.

Pavlović, M., Marković, Z., Veljković, M. and Buđevac, D. (2013), "Bolted shear connectors vs. Headed studs behavior in push-out tests", *J. Constr. Steel Res.*, **88**, 134-149.

Qi, J., Wang, J., Li, M. and Chen, L. (2017), "Shear capacity of stud shear connectors with initial damage: experiment, FEM model and theoretical formulation", *Steel Compos. Struct., Int. J.*, **25**(1), 79-92.

Qureshi, J., Lam, D. and Ye, J. (2011a), "The influence of profiled sheeting thickness and shear connector's position on strength and ductility of headed shear connector", *Eng. Struct.*, **33**(5), 1643-1656.

Qureshi, J., Lam, D. and Ye, J. (2011b), "Effect of shear connector spacing and layout on the shear connector capacity in composite beams", *J. Constr. Steel Res.*, **67**(4), 706-719.

Tahmasebinia, F., Ranzi, G. and Zona, A. (2013), "Probabilistic three-dimensional finite element study on composite beams with steel trapezoidal decking", *J. Constr. Steel Res.*, **80**, 394-411.

Titoum, M., Mazoz, A., Benanane, A. and Ouinas, D. (2016), "Experimental study and finite element modelling of push-out tests on a new shear connector of I-shape", *Adv. Steel Constr.*, **12**(4), 487-506.

Veritas, D.N. (2013), "DNV-RP-C208: Determination of Structural Capacity by Non-linear FE Analysis Methods", *Det Norske Veritas*.

Viest, I.M. (1956), "Investigation of Stud Shear Connectors for Composite Concrete and Steel T-beams", *J. Proceedings*, **52**(4), 875-892.

Wang, T. and Hsu, T.T. (2001), "Nonlinear finite element analysis of concrete structures using new constitutive models", *Comput. Struct.*, **79**(32), 2781-2791.

Xu, C., Sugiura, K., Wu, C. and Su, Q. (2012), "Parametrical static analysis on group studs with typical push-out tests", *J. Constr. Steel Res.*, **72**, 84-96.

Zheng, S., Liu, Y., Yoda, T. and Lin, W. (2016a), "Parametric study on shear capacity of circular-hole and long-hole perfobond shear connector", *J. Constr. Steel Res.*, **117**, 64-80.

Zheng, S., Liu, Y., Yoda, T. and Lin, W. (2016b), "Shear behavior and analytical model of perfobond connectors", *Steel Compos. Struct, Int. J.*, **20**(1), 71-891.

CC